JACS
JOURNAL OF THE AMERICAN CHEMICAL SOCIETY
Article
pubs.acs.org/JACS

Mechanistic Variants in Gas-Phase Metal-Oxide Mediated Activation of Methane at Ambient Conditions

Jilai Li,[†,‡] Shaodong Zhou,[†] Jun Zhang,[§] Maria Schlangen,[†] Dandamudi Usharani,[∥] Sason Shaik,*[,⊥] and Helmut Schwarz*[,†]

[†]Institut für Chemie, Technische Universität Berlin, Straße des 17. Juni 135, 10623 Berlin, Germany
[‡]Institute of Theoretical Chemistry, Jilin University, Changchun 130023, People's Republic of China
[§]Institute of Theoretical Chemistry, University of Cologne, Greinstraße 4, 50939 Cologne, Germany
[∥]Department of Lipid Science, CSIR-Central Food Technological Research Institute, Mysore, 570 020, India
[⊥]Institute of Chemistry and the Lise-Meitner-Minerva Center for Computational Quantum Chemistry, The Hebrew University of Jerusalem, 91904 Jerusalem, Israel

Supporting Information

ABSTRACT: The C−H bond activation of methane mediated by a prototypical heteronuclear metal-oxide cluster, $[Al_2Mg_2O_5]^{\bullet+}$, was investigated by using Fourier transform ion cyclotron resonance mass spectrometry (FT-ICR-MS) in conjunction with high-level quantum mechanical calculations. Experimentally, hydrogen-atom abstraction from methane by the cluster ion $[Al_2Mg_2O_5]^{\bullet+}$ takes place at ambient conditions. As to the mechanism, according to our computational findings, both the proton-coupled electron transfer (PCET) and the conventional hydrogen-atom transfer (HAT) are feasible and compete with each other. This is in distinct contrast to the $[XYO_2]^+$ (X, Y = Mg, Al, Si) cluster oxide ions which activate methane exclusively via the PCET route (Li, J.; Zhou, S.; Zhang, J.; Schlangen, M.; Weiske, T.; Usharani, D.; Shaik, S.; Schwarz, H. *J. Am. Chem. Soc.* **2016**, *138*, 7973−7981). The electronic origins of the mechanistically rather complex reactivity scenarios of the $[Al_2Mg_2O_5]^{\bullet+}/CH_4$ couple were elucidated. For the PCET mechanism, in which the Lewis acid−base pair $[Al^+-O^-]$ of the cluster acts as the active site, a clear correlation has been established between the nature of the transition state, the corresponding barrier height, the Lewis acidity-basicity of the $[M^+-O^-]$ unit, as well as the bond order of the M^+-O^- bond. Also addressed is the role of the spin and charge distributions of a terminal oxygen radical site in the direct HAT route. The knowledge of the factors that control the reactivity of PCET and HAT pathways not only deepens our mechanistic understanding of metal-oxide mediated C−H bond activation but may also provide guidance for the rational design of catalysts.

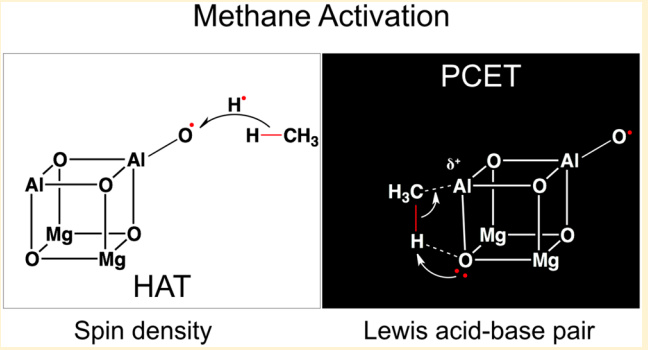

1. INTRODUCTION

The conversion of cheap and abundantly available methane to more valuable commodities constitutes one of the central challenges for solving some of the global energy problems,[1,2] and selective cleavage of the thermodynamically strong and kinetically inert C−H bond of methane under ambient conditions continues to capture much attention. Great efforts have also been spent to uncover the elementary steps and the mechanisms associated with these transformations.

Metal oxides, capable of bringing about activation of methane under single collision-conditions in the gas phase,[3] have served as prototypical systems to probe the active sites in heterogeneous catalysis, the so-called "aristocratic atoms".[4,5] Further, metal-oxide mediated hydrogen-atom transfer (HAT) from CH_4 to generate $CH_3^{\bullet}$ is viewed as a decisive step in the oxidative coupling of methane (OCM).[6−11]

Conceptually, there exist several mechanisms for the C−H bond activation of methane by a reactive metal oxide (Scheme 1).[1,8,12] In the conventional HAT process,[13−15] a hydrogen atom is transferred directly to an oxygen site that provides an electron hole, i.e., an oxyl radical ($O^{\bullet}$); concomitantly, in the homolytic cleavage of the C−H bond a methyl radical is released, Scheme 1a.[13,14] If the metal center is sufficiently carbophilic, a metal-assisted HAT may occur, resulting in a $[H_3C-M-O-H]$ intermediate, Scheme 1b. For these two mechanistic scenarios, quite a few examples do exist.[12,13] For metal oxides lacking a significant spin density at the accepting oxygen atom, in order to allow a direct HAT, a "prepared state" needs to be created, Scheme 1c.[13,14] This can be achieved, for example, by decoupling of the M═O double bond along the

Received: July 13, 2016
Published: August 12, 2016

DOI: 10.1021/jacs.6b07246
J. Am. Chem. Soc. 2016, 138, 11368−11377

Scheme 1. Mechanistic Scenarios for Metal-Oxide Mediated C−H Bond Cleavage of Methane

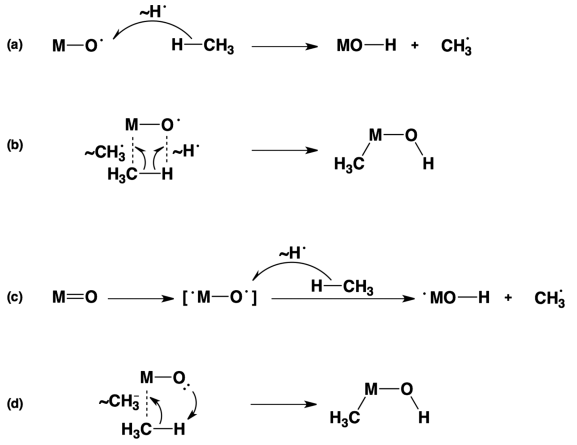

reaction coordinate; as this step is energy demanding, HAT is rather sluggish and often requires substrates having an activated C−H bond.[16−18] Finally, Scheme 1d depicts a proton-coupled electron transfer (PCET)[13−15,17,19−44] mechanism mediated by a Lewis acid−base pair $[M^+-O^-]$ serving as the active site of the catalyst. Here, a proton is abstracted from methane by the Lewis base O^- while the methyl anion is transferred to the Lewis-acidic metal center, thus forming a Grignard-type intermediate.[19,45,46] While scenarios (a)-(c) afford a *homolytic* C−H bond cleavage, the PCET mechanism (Scheme 1d) constitutes its *heterolytic* counterpart.

Generally speaking, these aforementioned mechanisms may be competitive and, therefore, can take place simultaneously. In practice, many factors, such as the effects of solvent, counterions, aggregations, surface defects, and so on, that prevail in homogeneous or heterogeneous catalysis, play an important role and a comprehensive understanding of the reaction is often lacking. Consequently, the unambiguous identification of the active sites and a proper characterization of their intrinsic properties as well as a clear-cut mechanistic assignment are hampered if not precluded. This holds true in particular for the study of methane activation under working conditions; here, the nature of the active center, the structure−activity relationship etc. are often shrouded in mystery, and mechanistic aspects continue to evoke fierce debates.[6,11,45,47−54] Since gas-phase experiments are not obscured by these difficult-to-control or poorly defined factors, well-designed studies on "isolated" reactants when combined with adequate computational work provide an ideal arena for experimentally probing the energetics and kinetics of a chemical reaction in an unperturbed environment at a strictly molecular level.[55−59] In fact, over the last years, numerous gas-phase studies have been conducted to uncover mechanistic aspects of bond activation by employing well-defined cluster oxides and subjecting them to single-collision experiments with the organic substrate.[60] Thus, molecular level-based knowledge has been provided which may prove helpful in the development of new concepts for the design of catalysts.[58,61−64]

The role of basic or acidic properties of metal oxides on the OCM has already formed the subject of detailed discussions,[6,65] but so far consensus has not been reached. In an exhaustive review by Zavyalova et al. covering more than 2700 research articles and about 140 patents on the topic of OCM by metal oxides, it was concluded that "*all oxides of the selected elements, which positively affect the selectivity to C_2 products, show strong basicity*".[48] In addition, it has been argued that the relative energies of the transition states for the heterolytic X−H cleavage (X = C, H) of CH_4 and H_2 can be rationalized in terms of both the different gas-phase acidities of CH_4 and H_2 and the basicity of the active sites which play a determining role.[65−68] However, in contrast to the extensive studies on the basicity effect, the role of the acidic site of the metal oxides has received much less attention.[6,69]

In a combined theoretical/experimental approach, we demonstrated recently that the heterolytic cleavage of the C−H bond of methane benefits not only from the basicity of oxygen, but also from the acidity of aluminum.[19] Thus, following a PCET mechanism, the strong Lewis acidic Al^+ and the basic O^- of the $[Al^+-O^-]$ active site of the cluster act in cooperation. It was found that significant charge densities effectively polarize the nearly nonpolar C−H bond in the initial stage of the process. Subsequently, the Al^+ site forms a new Al−CH_3 bond, concomitant with transfer of the proton to the O^- site, thus generating an O−H bond, as depicted in Scheme 1d. Further, the computational study demonstrated for a series of homo- and heteronuclear oxide-cluster ions $[XYO_2]^+$ (X, Y = Mg, Al, Si) that the relative energies of the rate-limiting transition states are controlled by both the Lewis acidity of the metal and the Lewis basicity of the oxygen atom of the active sites.[19]

As shown earlier, "doping" a free cluster in a designed way not only permits to control its chemistry but also to systematically change mechanistic details; consequently, fundamental scientific questions can be addressed.[12,70] For example, "doping" the $[Mg_2O_2]^{\bullet+}$ cluster with Ga_2O_3 changes the reactivity toward C−H bond activation dramatically: while the $[Ga_2Mg_2O_5]^{\bullet+}$ cluster abstracts a hydrogen atom even from methane under ambient conditions,[71] C−H bond activation by the homonuclear cluster $[Mg_2O_2]^{\bullet+}$ is only observed with those substrates having weaker C−H bonds.[72,73]

Herein, we report our findings on the thermal activation of methane by the heteronuclear oxide cluster $[Al_2Mg_2O_5]^{\bullet+}$ probed under single-collision conditions using Fourier transform ion cyclotron resonance mass spectrometry (FT-ICR-MS) and augmented by high-level quantum chemical calculations. We chose this species on the following grounds: (i) Magnesium oxides are of special interest not only in the present context, but also because they serve as superb, catalytically active metal oxides.[45,72,74] Also, aluminum oxides are of interest because γ-Al_2O_3 is broadly used as a catalyst or catalyst support in numerous industrial chemical transformations.[46,65,75,76] (ii) In our previous study,[19] among the series of oxide cluster ions $[XYO_2]^+$ (X, Y = Mg, Al, Si), the heteronuclear oxide $[AlMgO_2]^+$ was found to exhibit the lowest barrier for the PCET reaction with methane. As will be shown, the lowest-energy structure of $[Al_2Mg_2O_5]^{\bullet+}$ contains two $[AlMgO_2]$ units (see A01 in Scheme 2). (iii) Finally, this heteronuclear cluster can be regarded either as $[Mg_2O_2]^{\bullet+}$[72,73] doped with Al_2O_3 or as $[Al_2O_3]^{\bullet+}$[77] doped with Mg_2O_2, respectively; the reactivities of the two homonuclear cationic oxides have been investigated previously. In addition to systematically explore and compare the reactivity patterns of all the four mechanistic scenarios depicted in Scheme 1, in the present experimental/computational exercise we shall address the following aspects: *i*) the role of doping effects, *ii*) the correlation between the Lewis acidity and basicity of the Lewis acid−base $[M^+-O^-]$ unit and the activation energy, and *iii*) the determining factors that drive the

DOI: 10.1021/jacs.6b07246
J. Am. Chem. Soc. 2016, 138, 11368−11377

Scheme 2[a]

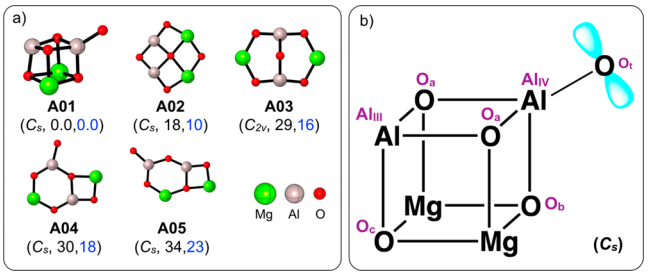

[a](a) The most stable isomers of $[Al_2Mg_2O_5]^{\bullet+}$ clusters; symmetries and relative enthalpies (kJ mol^{-1}) are given in parentheses: numbers in black are calculated at the G4 level of theory, and values in blue are calculated at the CCSD(T)-F12/aug-cc-pVTZ//MP2/cc-pVTZ level of theory. (b) Schematic doublet ground-state structure of A01. The charge is omitted for the sake of clarity. The cyan isosurface indicates the spin-density distribution.

reaction to proceed through a conventional HAT versus a PCET pathway.

2. RESULTS AND DISCUSSION

The Fourier transform ion-cyclotron resonance (FT-ICR) mass spectra for the reactions of mass-selected, thermalized $[Al_2Mg_2{}^{18}O_5]^{\bullet+}$ ions (m/z = 192) with the isotopologues of methane (see Experimental Details) are given in Figure 1;

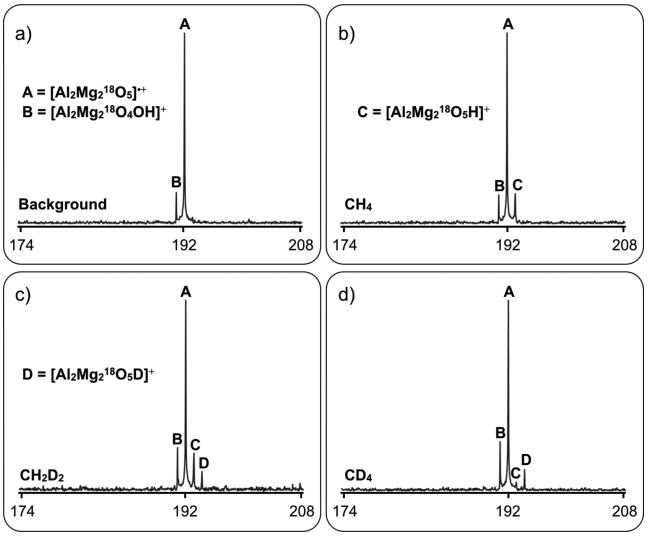

Figure 1. Mass spectra for the thermal reactions of $[Al_2Mg_2{}^{18}O_5]^{\bullet+}$ with (a) background gases at a pressure of 6.0 × 10^{-10} mbar after a reaction time of 3s, (b) CH_4 and (c) CH_2D_2, at a pressure of 1.0 × 10^{-7} mbar after a reaction time of 3s, (d) CD_4 at a pressure of 1.0 × 10^{-7} mbar after a reaction time of 5 s, respectively. The unit for the x axes is m/z.

spectra of the reactions with background impurities as well as with argon as an inert substrate have also been recorded to serve as a reference. As shown in Figure 1a, a signal with Δm = −1 appears relative to the precursor ion $[Al_2Mg_2{}^{18}O_5]^{\bullet+}$; this signal can be assigned to the product ion $[Al_2Mg_2{}^{18}O_4{}^{16}OH]^+$ which originates from an $^{18}O/^{16}OH$ exchange process between the cluster ion $[Al_2Mg_2{}^{18}O_5]^{\bullet+}$ and background water, reaction 1.

A hydrogen-atom abstraction product $[Al_2Mg_2{}^{18}O_5H]^+$ is clearly identified when CH_4 is admitted to the ICR cell at a stationary pressure of 1.0 × 10^{-7} mbar; Figure 1b, reaction 2, and the C−H bond scission was confirmed in isotopic labeling experiments. For example, $[Al_2Mg_2{}^{18}O_5D]^+$ ions are generated from CD_4 under the concomitant elimination of $CD_3^{\bullet}$, reaction 3. The compositions of all ionic species $[Al_2Mg_2{}^{18}O_4{}^{16}OH]^+$, $[Al_2Mg_2{}^{18}O_5H]^+$, and $[Al_2Mg_2{}^{18}O_5D]^+$ have been confirmed in high-resolution measurements.

The rate coefficient for the hydrogen-atom abstraction from CH_4 has been estimated to 3.6 × 10^{-12}cm^3 molecule^{-1} s^{-1}; this corresponds to a collision efficiency (ϕ) of 0.4%, relative to the collision rate.[78−80] The intramolecular kinetic isotope effect (KIE) derived from the $[Al_2Mg_2{}^{18}O_5]^{\bullet+}/CH_2D_2$ couple, Figure 1c, reactions 4a, 4b), amounts to $KIE_{C-H/C-D}$ = 2.0.

Summarizing the experimental findings, it is clear that $[Al_2Mg_2{}^{18}O_5]^{\bullet+}$ activates methane under thermal, single-collision conditions.

$$[Al_2Mg_2{}^{18}O_5]^{\bullet+} + H_2{}^{16}O \rightarrow [Al_2Mg_2{}^{18}O_4{}^{16}OH]^+ + {}^{18}OH^{\bullet} \quad (1)$$

$$[Al_2Mg_2{}^{18}O_5]^{\bullet+} + CH_4 \rightarrow [Al_2Mg_2{}^{18}O_5H]^+ + CH_3^{\bullet} \quad (2)$$

$$[Al_2Mg_2{}^{18}O_5]^{\bullet+} + CD_4 \rightarrow [Al_2Mg_2{}^{18}O_5D]^+ + CD_3^{\bullet} \quad (3)$$

$$[Al_2Mg_2{}^{18}O_5]^{\bullet+} + CH_2D_2 \rightarrow [Al_2Mg_2{}^{18}O_5H]^+ + CHD_2^{\bullet} \quad (4a)$$

$$[Al_2Mg_2{}^{18}O_5]^{\bullet+} + CH_2D_2 \rightarrow [Al_2Mg_2{}^{18}O_5D]^+ + CH_2D^{\bullet} \quad (4b)$$

In order to obtain mechanistic insight, high-level quantum mechanical (QM) calculations were carried out. Since the reactivity pattern turned out to be rather complex, we confine our discussion to key results in the main text; for additional details, see the Supporting Information (SI).

The most stable structure of $[Al_2Mg_2O_5]^{\bullet+}$ corresponds to A01; it has a cage-like geometry with a terminal oxygen atom (O_t), at which the spin density is located. The electronic ground state of the cluster oxide has a doublet configuration with the quartet state higher in energy by 303 kJ mol^{-1} (Scheme 2, and Table 1). The terminal oxygen in A01 is coordinated to a fourfold coordinated Al_{IV} atom which, together with a threefold coordinated Al_{III} atom, is located on the upper face of the quasi-cubic cell; the Al_{III} atom is connected to the Al_{IV} atom via two threefold coordinated oxygen atoms, O_a. The two magnesium atoms are located at the

Table 1. NBO Charge and Spin Density Distributions of the Cluster Ion A01[a]

	spin	charge
O_t	1.01	−0.64
O_a	0.00	−1.51
O_b	0.00	−1.65
O_c	0.00	−1.62
Al_{III}	0.00	2.17
Al_{IV}	−0.01	2.03
Mg	0.00	1.87

[a]See Scheme 2b for the atom code.

DOI: 10.1021/jacs.6b07246
J. Am. Chem. Soc. 2016, 138, 11368−11377

bottom of the cube; due to the C_s symmetry of the cluster, both magnesium atoms are equivalent as are the bridging oxygen atoms O_a. The two magnesium atoms are linked by the oxygen atoms O_b and O_c, which also connect the lower and the upper faces of the cube. We note that the core of this structure resembles closely that of the cubane-shaped $LiMg_3O_4$ and Mg_4O_4 clusters; the latter have been discussed as mimics for lithium-doped magnesium oxides.[81,82]

As shown in Scheme 2, there exist in A01 several potential reactive sites and routes for methane activation. In our calculations, we considered H atom abstraction by the oxygen atoms O_t, O_a, O_b, and O_c, with or without the formation of metal−carbon bonds (pathways A−D and E−J, respectively, Scheme 3). The relative energies of the corresponding transition states (TSs) are summarized in Table 2; for schematic representations of the various transition-state geometries, see Scheme 3. We should note that the binding of methyl group to the Al_{IV} atom is much weaker; test calculations confirmed that the reaction channel corresponding to a transfer of the methyl group to the 4-fold coordinated Al_{IV} atom is unfavorable.

Since the unpaired electron of A01 is localized at the terminal oxygen atom $O_t^{\bullet-}$, this site is expected to be engaged in a conventional HAT reaction.[13,83,84] This is, indeed, confirmed by the calculations: HAT to $O_t^{\bullet-}$ can proceed at thermal, single-collision conditions with a negative apparent barrier (−4 kJ mol^{-1}, pathway A). Not surprisingly, prohibitively high barriers are encountered in the HAT to the oxygen atoms having no spin density, i.e., O_a, O_b, and O_c, in pathways B, C, and D. However, though not unexpectedly, H-abstraction by $O_t^{\bullet-}$ is rather unfavorable when in concert the Al_{III} atom forms an Al−C bond to the methyl group (pathway E). In contrast, HAT by O_a, O_b, and O_c is much less impeded when this step is coupled with forming a metal−carbon bond to an adjacent aluminum atom (pathways F−J versus B−D). We note that no transition states have been located for making a Mg−C bond; according to relaxed scan calculations, the Mg−C bond is cleaved leading to TS-O_t instead.

In the following, we will discuss in more detail pathways A and G; both, on their doublet ground state surfaces, possess negative apparent energy barriers, Figure 2.[74] In consideration of the uncertainty of the theoretical methods (a few kJ mol^{-1}), pathway F is also feasible under thermal, single-collision conditions, as the rate-limiting step, TS-Al/O_a, is rather similar to TS-Al/O_c of pathway G. For the sake of clarity, details of the former as well as of all other remaining pathways, considered in this study, are transferred to the SI (Figure S1 and Scheme S1).

Let us consider first the conventional HAT to $O_t^{\bullet-}$, pathway A, which commences with generating an encounter complex, EC1, from the separated reactants A01 and CH_4 (SR). EC1 is stabilized by an electrostatic interaction between the incoming hydrocarbon substrate and the magnesium site; this step is exothermic by 64 kJ mol^{-1}. Next, one C−H bond of methane is activated and the hydrogen atom is transferred to the $O_t^{-\bullet}$ unit of EC1 via transition state TS-O_t; the latter is located 4 kJ mol^{-1} below the entrance channel. Completion of the C−H bond cleavage results in the formation of intermediate I1 (−101 kJ mol^{-1}); in I1 the methyl radical is loosely coordinated to the cluster via the hydrogen-atom of the newly formed OH group. Finally, the hydroxide product ion P1 is generated under the liberation of the methyl radical. The structures of the stationary points along pathway A resemble closely to that of a

Scheme 3. Various Pathways (A− J) for the C−H Bond Activation Mediated by Cluster Ion A01 As Calculated at the B2GP-PLYP/def2-TZVP Level of Theory[a]

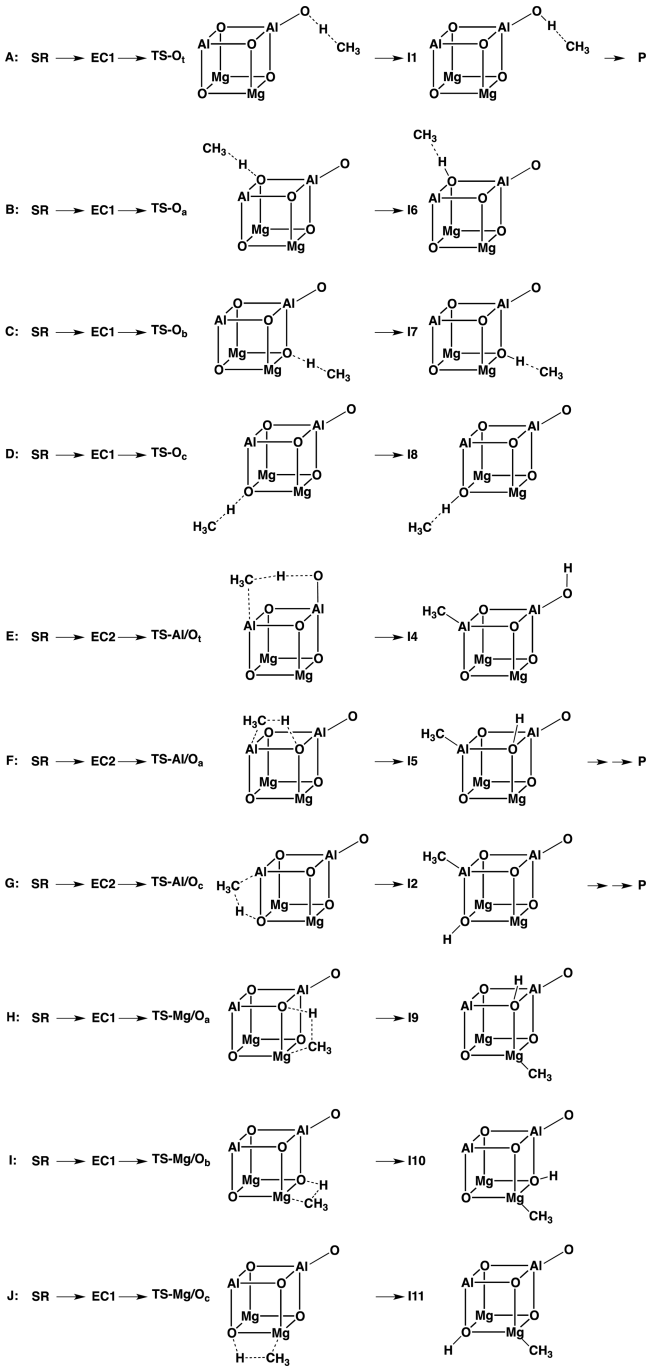

[a]SR refers to the separated reactants A01 and CH_4; EC1 and EC2 denote the encounter complexes.

radical mechanism as described before for HAT reactions.[13,14,17,71,85,86]

As to pathway G, the reaction starts with the formation of a rather stable encounter complex, EC2; this barrier-free step is exothermic by 92 kJ mol^{-1}. Notably, EC2 is significantly stabilized by a strong electrostatic interaction between the Lewis acidic Al_{III} coordination site (δ^+) and the Lewis basic carbon atom (δ^-) of methane; the H···C···Al triad in EC2 is linearly arranged with the lobe of the σ orbital of the C−H

DOI: 10.1021/jacs.6b07246
J. Am. Chem. Soc. 2016, 138, 11368−11377

Table 2. Relative Energies (ΔH, kJ mol^{-1}) of the Transition State for the First Hydrogen-Atom Abstraction in the Pathways A–J for the Reactions of A01 with CH_4 As Calculated at the B2GP-PLYP/def2-QZVPP//B2GP-PLYP/def2-TZVP Level of Theory

pathway	TS	ΔH
A	TS-O_t	−6.0 (−4.3[a])
B	TS-O_a	226.4
C	TS-O_b	185.7
D	TS-O_c	175.1
E	TS-Al/O_t	95.3
F	TS-Al/O_a	−3.1 (3.1[a])
G	TS-Al/O_c	−7.3 (−4.8[a])
H	TS-Mg/O_a	69.0
I	TS-Mg/O_b	53.3
J	TS-Mg/O_c	50.2

[a]Single-point energies calculated at the CCSD(T)/CBS-[VTZ:VQZ]//B2GP-PLYP/def2-TZVP level of theory. See Scheme 3 for the details.

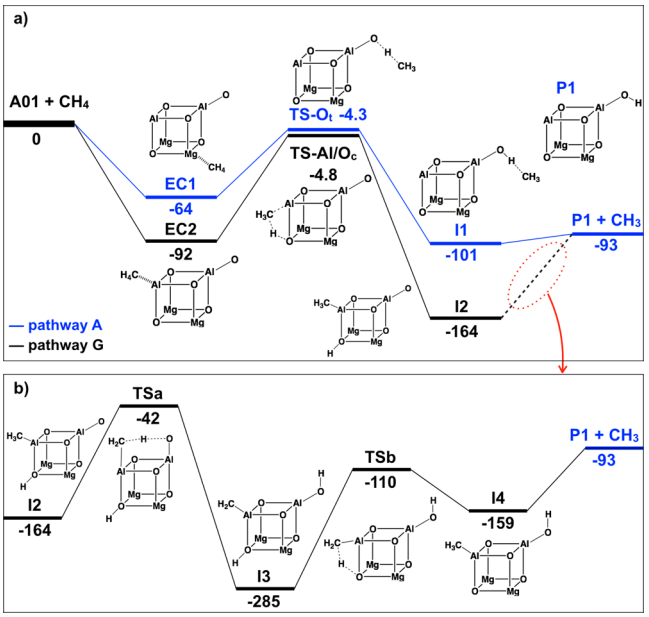

Figure 2. Potential energy profiles (ΔH, kJ mol^{-1}) and schematized key ground-state structures involved in the reaction of A01 with CH_4. (a) Overview of the reaction; (b) detailed reaction sequence from intermediate I2 to the separated product P1 and the methyl radical. All relative energies, except TS-O_t and TS-Al/O_c, are calculated at the B2GP-PLYP/def2-QZVPP//B2GP-PLYP/def2-TZVP level; TS-O_t and TS-Al/O_c are based on the CCSD(T)/CBS[VTZ:VQZ]//B2GP-PLYP/def2-TZVP calculations. The energies are corrected by ZPVE contributions. For details, see the SI.

bond interacting with the aluminum atom. Subsequently, C–H bond cleavage takes place at the $[Al^{+}_{III}–O^{-}_{c}]$ unit of EC2; the hydrogen atom is transferred to the oxygen site O^{-}_{c} via transition state TS-Al/O_c; the latter is located 5 kJ mol^{-1} below the separated reactants. After passing TS-Al/O_c, a quite stable intermediate I2 is generated, lying 164 kJ mol^{-1} below the reaction entrance. Next, as shown in Figure 2b, rather than splitting the Al–C bond directly, the reaction proceeds by a series of hydrogen-atom-shifts, i.e. I2 → TSa → I3 → TSb →I4, to generate the final products P1 and $CH_3^{\bullet}$. Indeed, pathway G can be described as a *heterolytic* cleavage of the C–H bond of methane mediated by the Lewis acid–base pair $[Al^{+}–O^{-}]$ of the cluster ion; the basic oxygen O^{-}_{c} abstracts the hydrogen atom as a proton, while the CH_3 moiety moves with its electron pair as a methyl anion CH_3^{-} to generate a covalent bond with the positively charged Lewis acidic Al^{+}_{III}. The rate-determining step corresponds to the activation of the C–H bond via transition state TS-Al/O_c, which is also accessible under ambient conditions.

Both mechanistic scenarios of C–H bond cleavage by either the radical oxygen atom in pathway A or the Lewis acid–base pair $[Al^{+}_{III}–O^{-}_{c}]$ in pathway G have in common that cleavage of the C–H bond constitute the rate-limiting step; thus, in line with the experimentally findings a KIE > 1 has been observed.

To understand the origins of the respective barriers of the various pathways summarized in Table 2, we examined the correlation of the deformation energy (ΔE_{def}) required for the geometric distortion of the reactants on way to their TSs with the respective reaction barrier ($\Delta E^{\ddagger}$), Figure 3; this was done

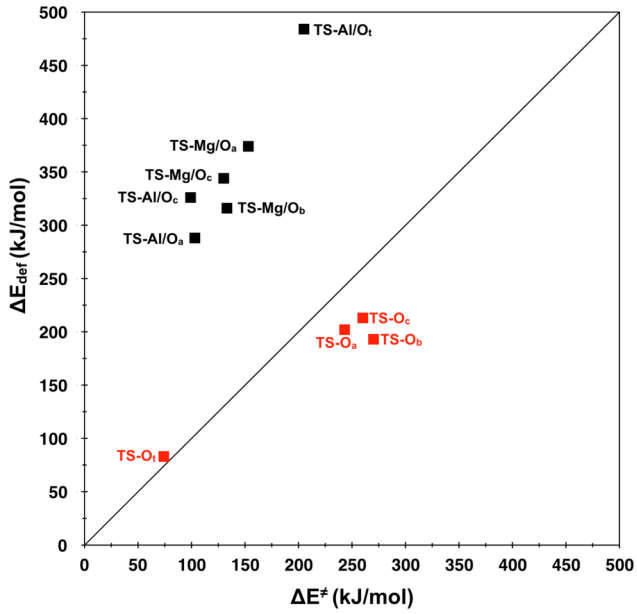

Figure 3. Plot of the sum of the deformation energies of the reactants in the TS (ΔE_{def}, kJ mol^{-1}) versus the corresponding barriers $\Delta E^{\ddagger}$ (kJ mol^{-1}) relative to the encounter complexes, for the TSs corresponding to the first C–H bond activation in pathways A–J. The line is drawn with a slope of unity such that $\Delta E_{def} = \Delta E^{\ddagger}$ while the vertical distance from the line gauges the interaction energy between the deformed reactants at the TSs. The black squares correspond to a PCET mechanism, while the red squares correspond to a HAT mechanism.

for all the pathways using the energy decomposition analysis according to which the barrier for HAT is composed of ΔE_{def} and the interaction energy between the deformed reactants in the TS.[87–99] According to previous studies, a plot of ΔE_{def} against $\Delta E^{\ddagger}$ serves as a simple diagnostic of the HAT/PCET dichotomy.[87,88] Thus, the plots of ΔE_{def} against $\Delta E^{\ddagger}$ are located near the line $\Delta E_{def} = \Delta E^{\ddagger}$ for pathways A, B, C, and D; this indicates that the deformation energy alone accounts for the reaction barrier and, as shown before, this correlation can be assigned to HAT pathways.[87,88] By contrast, for pathways E–J, we note $\Delta E_{def} \gg \Delta E^{\ddagger}$; this shows that the TSs of all these pathways are stabilized by attractive interactions between the deformed reactants. These significant stabilizing interactions in the TSs reflect their multicentered bonding as well as their

DOI: 10.1021/jacs.6b07246
J. Am. Chem. Soc. 2016, 138, 11368–11377

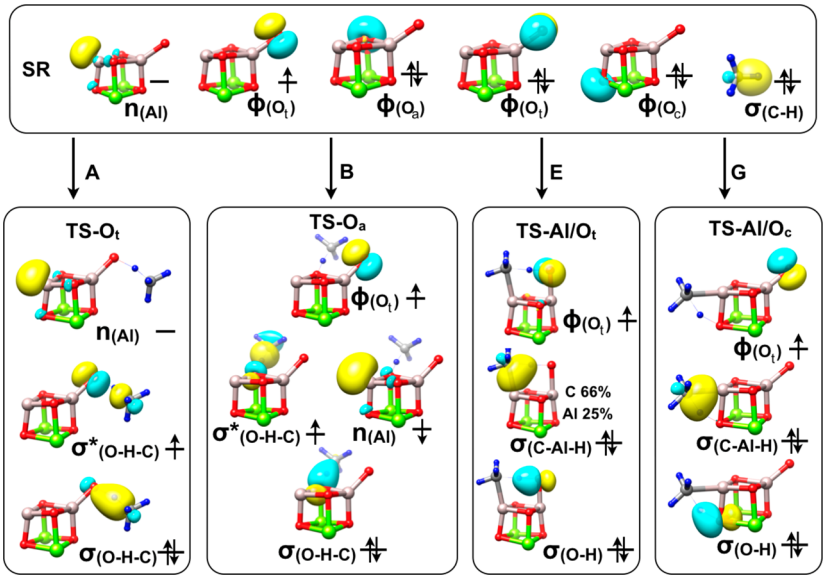

Figure 4. Schematic orbital diagrams represented by QROs (quasi-restricted orbitals) for separated reactants SR, and TS in the HAT (A and B) and PCET (E and G) pathways. Only representative orbitals are shown for the transition states.

ionic character, which brings about electrostatic and bonding stabilization and thus lowers the energy of the transition state for PCET pathways.[14,17,19,87,88] We note that the largest stabilization is observed for pathway E proceeding through TS-Al/O_t. As discussed below, the mechanism of C−H activation via TS-Al/O_t does not correspond to a conventional HAT reaction even though an oxyl radical $O_t^{-\bullet}$ serves as the reactive site.

Further, in order to obtain complementary and insightful information regarding a distinction between HAT versus PCET, the electronic structures of the TSs were analyzed.[18,85,86,100−104] Figure 4 shows the orbitals that participate in the chemical transformation for the pathways A, B, E, and G; for the remaining pathways, this information is provided in SI, Figure S2.

First we consider the electronic structures of A01 and CH_4, as shown in Figure 4. The precursor ion A01 possesses an empty orbital on Al^+_{III}, $n_{(Al)}$, a singly occupied orbital localized on the terminal oxygen, $\Phi_{(Ot)}$, and three doubly occupied orbitals accommodating the lone-pair electrons of the oxygen atoms O_t, O_a, and O_c; orbitals with electrons of O_b are not involved in the reactions. One of the four doubly occupied $\sigma_{(C-H)}$ orbitals from methane is also given.

As mentioned, pathway A can be described in terms of a standard HAT mechanism. As shown in Figure 4A, three electrons are delocalized over the O−H−C moiety in transition state TS-O_t; one of the electrons is contributed by the $O_t^{-\bullet}$ radical ($\Phi_{(Ot)}$ in SR), and two by the $\sigma_{(C-H)}$ bond of methane. Thus, TS-O_t is characterized by a 3-electron/3-center bond with a doubly occupied bonding orbital along the O−H−C axis, $\sigma_{(O-H-C)}$, and a singly occupied antibonding orbital, $\sigma^*_{(O-H-C)}$, with a node on the H atom in transit. The empty orbital $n_{(Al)}$ of Al^+_{III} acts as a spectator herein.

In contrast, the unpaired electron of the $O_t^{-\bullet}$ radical is not involved in the HAT process of pathway B (Figure 4B). Here, one of the lone-pair electrons of O_a shifts to the empty orbital $n_{(Al)}$ where it increases spin density of Al from 0.00 to −0.64 (see Table S2). This leads to have electron hole on O_a, which then serves as a H atom acceptor as is typical for a standard HAT. However, this process, which involves high-penalty due to the requisite electronic reorganization, leads to a high barrier located 226 kJ mol^{-1} above the energy of the entrance channel. Obviously, this pathway is not accessible under thermal conditions. The same holds true for pathways C and D (see Figure S2); here a β-electron is shifted from a doubly occupied orbital of the *spin-free* oxygen atoms O_b, or O_c, so as to create an electron hole to facilitate the subsequent HAT from methane.

Next, we consider pathway E. As shown in Figure 4E, the electron pair from the $\sigma_{(C-H)}$ bond of methane is donated into the empty orbital $n_{(Al)}$ of the Al^+_{III} atom of the cluster, resulting in the formation of a new $\sigma_{(C-Al-H)}$ bond. Then, the remaining proton in transit is captured by the doubly occupied $\Phi_{(Ot)}$ orbital of the terminal oxygen atom $O_t^{-\bullet}$, thus generating a $\sigma_{(O-H)}$ bond in the intermediate. However, an electronic reorganization of the singly- and doubly occupied $\Phi_{(Ot)}$ orbitals in SR is required for the formation of the $\sigma_{(O-H)}$ bond; this gives rise to a high energy barrier TS-Al/O_t (95 kJ mol^{-1}). Since the locations to which the proton and the electron are transferred differ,[13] pathway E can be assigned to a PCET rather than a HAT, even though an $O_t^{-\bullet}$ radical serves as the reactive site.[13,14] In addition, the negative charge on the carbon atom increases significantly from −1.00 in isolated CH_4 to −1.27 (Table S2), indicating that the electron does not transfer simultaneously along with the proton in this process.

Pathways F−J have the features of a *heterolytic* cleavage of the C−H bond of methane via a PCET process. In the following, pathway G is discussed as a representative example. As shown in Figure 4G, the electron pair from the $\sigma_{(C-H)}$ bond of methane in SR, is accepted by the empty orbital $n_{(Al)}$ of the Al^+_{III} atom of the cluster in SR, forming a mixed $\sigma_{(C-Al-H)}$ bond in TS-Al/O_c. Further, the proton is captured by the doubly occupied $\Phi_{(Oc)}$ orbital of oxygen atom O_c in SR. Thus, a $\sigma_{(O-H)}$ and a $\sigma_{(Al-C)}$ bond are created in the intermediate; in the former the two electrons originate from the doubly occupied $\Phi_{(Oc)}$ orbital of the cluster and in the latter from the $\sigma_{(C-H)}$ bond of methane (see SR in Figure 4). The analysis of the NBO-calculated spin and charge distributions (Table S2) indicates that an unpaired electron is not located on the hydrogen abstracting oxygen atom O_c; instead, significant

DOI: 10.1021/jacs.6b07246
J. Am. Chem. Soc. 2016, 138, 11368−11377

negative charges are generated on O_c and the carbon atom in TS-Al/O_c; the former facilitates the C−H bond activation by proton abstraction and the latter is beneficial to create the Al−CH_3 bond. As a result, TS-Al/O_c is significantly stabilized, and even lies lower in energy than TS-O_t, in which the oxyl unit $O_t^{-\bullet}$ serves as the H-abstractor for enabling a conventional HAT.

As noted earlier,[105,106] an increasing spin density and a decreasing negative charge on the hydrogen-abstracting oxygen atom favorably affect a HAT reaction, with the consequence that even methane can be activated.[71] As shown in Tables 1 and 2, we can see that a less negative charge, as well as a significant spin on the reactive oxygen atom are beneficial for a conventional HAT reaction (pathways A); in contrast, a significantly negative charge on the reactive, spin-free oxygen atoms results in prohibitively high barriers (pathways B−D).

Quite interestingly, inspection of the NBO charge of the Lewis acid−base pair $[M^+-O^-]$ (M = Al, Mg) of the cluster ion reveals a correlation with the relative energies of the TSs in PCET pathways E to J. Indeed, a clear correlation between the nature of TS, its barrier and the Lewis acidity−basicity of the $[M^+-O^-]$ unit serving as the reactive site can be established: the more acidic the metal and the more basic the oxygen atoms are in the $[M^+-O^-]$ unit (Table 1), the stronger stabilized is the corresponding TS in a PCET reaction.

A comparison between the $[Al_2Mg_2O_5]^{\bullet+}/CH_4$ couple and the $[Al_2O_3]^{\bullet+}/CH_4$ pair described previously[77] reveals a striking doping effect.[70] The Al(μ-O)$_2$AlO$_t$ of $[Al_2O_3]^{\bullet+}$ is also present in A01; here the $[Mg_2O_2]$ unit acts as a dopant. The corresponding rate constant $k([Al_2O_3]^{\bullet+}/CH_4)$ amounts to 7.0×10^{-11} cm^3 molecule^{-1} s^{-1} with an efficiency of around 7%.[77] Thus, the reactivity of $[Al_2O_3]^{\bullet+}$ toward CH_4 is an order of magnitude higher than that of the $[Al_2Mg_2O_5]^{\bullet+}/CH_4$ couple. Therefore, doping the cluster ion $[Al_2O_3]^{\bullet+}$ with Mg_2O_2 decreases its reactivity. However, "doping" increases the chemoselectivity as the competing conversion of methane into formaldehyde becomes unfavorable for the heteronuclear cluster oxide. As to the mechanistic implications, a sizable barrier (TS-O_t) in pathway A of the doped system is encountered, while a barrier-free hydrogen-atom abstraction occurs in the $[Al_2O_3]^{\bullet+}/CH_4$ couple.[77] As a PCET pathway had not been considered in the previous study on the $[Al_2O_3]^{\bullet+}/CH_4$ couple,[77] thus, we recalculated the PCET pathway for comparison. The corresponding TS-Al/O_a for the $[Al_2O_3]^{\bullet+}/CH_4$ couple is located 65 kJ mol^{-1} below the entrance channel (Figure S3), in sharp contrast to the corresponding value of 3 kJ mol^{-1} found in pathway F of the A01/CH_4 couple. The significant HAT barrier of the doped system compared to that of the $[Al_2O_3]^{\bullet+}/CH_4$ couple can be ascribed to a larger bond order between the terminal oxygen and the Al atom: the calculated Wiberg bond index (WBI) of the Al−O_t bond in A01 amounts to 0.60, whereas a value of 0.34 is obtained for the corresponding bond in $[Al_2O_3]^{\bullet+}$ (Table S1). The same holds true for the PCET transition state TS-Al/O_a: the WBI of the Al_{II}-O_a bond in the active site of $[Al_2O_3]^{\bullet+}$ corresponds to 0.30, whereas this value amounts to 0.45 for that Al_{III}-O_a bond in $[Al_2Mg_2O_5]^{\bullet+}$. These findings imply that metal oxides possessing a more ionic nature of the $[M^+-O^-]$ unit have a smaller apparent activation energy for the C−H bond activation of methane and favor PCET pathway.

3. CONCLUSIONS

In summary, we investigated mechanistic variants and their electronic origins for the reactions of the heteronuclear oxide cluster $[Al_2Mg_2O_5]^{\bullet+}$ with CH_4 by using the FT-ICR-MS experiments and high-level QM calculations. First, HAT from methane to the cluster ion A01 proceeds under thermal, single-collision conditions. Second, as shown computationally, both a proton-coupled electron transfer (PCET) mechanism and the conventional HAT route are feasible and competitive. To our knowledge this is the first example demonstrating that both mechanistic variants may coexist. In detail, the PCET reaction takes place on the Lewis acid−base pair $[Al_{III}^+-O_c^-]$; alternatively, the terminal oxygen $O_t^{-\bullet}$ abstracts a hydrogen-atom through the conventional HAT route. Third, a correlation between the nature of the TSs, the barriers and the Lewis acidity-basicity of the $[M^+-O^-]$ units serving as the reactive site has been established by a quantitative analysis of the NBO-calculated spin and charge distributions, as well as WBI. Fourth, the roles of the spin and charge distributions on the oxyl site of a terminal oxygen radical site in HAT processes are clarified. The present results may provide a valuable and general guidance for probing doping effects on the mechanisms of C−H bond activation and, thus, may prove useful in the rational design of catalysts.

4. METHOD

4.1. Experimental Details. The ion/molecule reactions were performed with a Spectrospin CMS 47X Fourier transform ion cyclotron resonance (FT-ICR) mass spectrometer equipped with an external ion source as described elsewhere.[107−109] In brief, $[Al_2Mg_2{}^{18}O_5]^{\bullet+}$ was generated by laser ablation of a Al/Mg (1:1) disk using a Nd:YAG laser operating at 1064 nm in the presence of $^{18}O_2$ (>99%) seeded in helium; the latter serves as carrier gas. $^{18}O_2$ was used to avoid ambiguities in the assignment of product species due to the generation of isobaric species in the course of the reactions with methane and background gases.

Using a series of potentials and ion lenses, the ions were transferred into the ICR cell, which is positioned in the bore of a 7.05 T superconducting magnet. After proper thermalization by pulsed-in argon (ca. 2×10^{-6} mbar), the reactions of mass-selected $[Al_2Mg_2{}^{18}O_5]^{\bullet+}$, m/z = 192, were studied by introducing isotopologues of methane, i.e., CH_4, CD_4, and CH_2D_2, via a leak valve at stationary pressures. A temperature of 298 K for the thermalized cluster ions was assumed.[107−109]

4.2. Computational Details. *Assignment of the Lowest-Energy Structure.* To obtain the lowest-energy structure of the cluster ion $[Al_2Mg_2{}^{18}O_5]^{\bullet+}$, a Fortran code based on a genetic algorithm (GA)[110] has been used to generate initial guess structures of the $[Al_2Mg_2O_5]^{\bullet+}$ clusters. The B3LYP/6-31G level of theory was employed in the GA calculations that produced more than 200 fully optimized structures without imposing any symmetry constrains.[111,112] Subsequently, more than 100 low-lying isomers were reoptimized at the G4 level of theory to obtain the global minimum structure of $[Al_2Mg_2O_5]^{\bullet+}$. In addition, the artificial bee colony (ABC) algorithm[113,114] was also employed by using the "'ABCluster'" software to search the global as well as the local minima; the B3LYP/def2-TZVP level of theory was used in these structural optimization. Finally, the five lowest-energy structures were reoptimized at the MP2/cc-pVTZ level of theory; the so-obtained structures were used for single-point energy calculations by employing advanced QM computational methods free of any empiricism, i.e., at the CCSD(T)-F12/AVTZ level of theory.[115] All these calculations were confined to the doublet cage-like structure A01. We note that the global minimum of the quartet state is located more than 140 kJ mol^{-1} above doublet A01.

Electronic Structure Calculations. The B2GP-PLYP[116] double hybrid density functional method in conjunction with the def2-TZVP

DOI: 10.1021/jacs.6b07246
J. Am. Chem. Soc. 2016, 138, 11368−11377

basis set were applied to optimize the structures of stationary points along the reaction coordinates. The influence of van der Waals effects has been studied by using the Gaussian 09 default of Grimme's empirical dispersion parameters.[117]

Harmonic vibrational frequencies were computed to verify the nature of the stationary points. The minimum structures reported in this paper show only positive eigenvalues of the Hessian matrix, whereas the transition states (TSs) have one negative eigenvalue. Intrinsic reaction coordinate (IRC)[118−121] calculations were also performed to confirm that the transition states correlate with the designated intermediates.

The zero-point vibrational energy (ZPVE) and thermal corrections to the enthalpy were calculated on structures optimized at the B2GP-PLYP/def2-TZVP level. The thermodynamic functions (ΔH) were estimated within the ideal gas, rigid-rotor, and harmonic oscillator approximations at 298 K and 1 atm.

To refine the energies, single-point energy (SPE) calculations were performed further at the B2GP-PLYP/def2-QZVPP level of theory. In order to obtain a chemical precision for the rate-limiting transition barriers, TS-O_t, TS-Al/O_c, and TS-Al/O_a, SPE calculations at the standard CCSD(T)/CBS[VTZ:VQZ] level of theory using the B2GP-PLYP/def2-TZVP structures were carried out.

Natural bond orbital (NBO)[122−127] calculations were performed to obtain further information on selected stationary points along the reaction coordinates.

Deformation energies (ΔE_{def}) were calculated at the B2GP-PLYP/def2-TZVP level for the respective transition states, and were plotted again the respective barriers ($\Delta E^{\ddagger}$) as a diagnostic tool.[87] ΔE_{def} is the energy spent by the reactants to reach the structure adopted in the transition state, respectively, namely, $\Delta E_{def} = E(CH_4 + [Al_2Mg_2{}^{18}O_5]^{\bullet+}$ at TS geometry) − E(EC), while the respective barriers are the electronic barrier without corrections for zero-point energy or any thermal contributions. To avoid negative barriers (see Table 2), the energy of the encounter complex was used as a reference state.

The barrier is related to the deformation energy as follows:

$$\Delta E^{\ddagger} = \Delta E_{def} + \Delta E_{int}$$

ΔE_{int} corresponds the total interaction energy, contributed by repulsive interactions (e.g., Pauli repulsion) and stabilizing interactions (electrostatic, polarization, and bonding). The line in the Figure 3 has a slope of unity with $\Delta E^{\ddagger} = \Delta E_{def}$. Large ΔE_{int} values indicate strong missing between the proton-transfer/electron-transfer states and the HAT states in the neighborhood of the TS.[14,17,87,128]

All density functional theory calculations were performed with the Gaussian 09 package,[129] and the coupled-cluster theory calculations were carried out by using Molpro2012.1.[130]

■ ASSOCIATED CONTENT

Supporting Information

The Supporting Information is available free of charge on the ACS Publications website at DOI: 10.1021/jacs.6b07246.

Additional potential energy surface, schematic molecular orbital diagrams, NBO-calculated charge and spin density, and Wiberg bond index mentioned in the main text, and Cartesian coordinates for all calculated species (PDF)

■ AUTHOR INFORMATION

Corresponding Authors

*Helmut.Schwarz@tu-berlin.de
*sason@yfaat.ch.huji.ac.il

Notes

The authors declare no competing financial interest.

■ ACKNOWLEDGMENTS

This research was sponsored by the Deutsche Forschungsgemeinschaft (DFG), in particular the Cluster of Excellence "Unifying Concepts in Catalysis" (coordinated by the Technische Universität Berlin and funded by the DFG), and the Fonds der Chemischen Industrie. The work at Jilin University has been supported by the National Natural Science Foundation of China (21473070). The work at the Hebrew University has been supported by the Israel Science Foundation (ISF Grant 1183/13). Dr. D. Usharani thanks the Lise Meitner-Minerva Center for computational facilities. We are grateful to Dr. Thomas Weiske, TU Berlin, for sharing with us his technical expertise. This article is dedicated to Professor Howard Alper, Ottawa, in recognition of his outstanding service as a "Science Diplomat".

■ REFERENCES

(1) Olivos-Suarez, A. I.; Szécsényi, À.; Hensen, E. J. M.; Ruiz-Martinez, J.; Pidko, E. A.; Gascon, J. *ACS Catal.* **2016**, *6*, 2965−2981.
(2) Olah, G. A.; Goeppert, A.; Prakash, G. K. S. *Beyond Oil and Gas: The Methanol Economy*; Wiley-VCH: Weinheim, Germany, 2006.
(3) Schröder, D.; Schwarz, H. *Angew. Chem., Int. Ed. Engl.* **1995**, *34*, 1973−1995.
(4) Taylor, H. S. *J. Phys. Chem.* **1925**, *30*, 145−171.
(5) Taylor, H. S. *Proc. R. Soc. London, Ser. A* **1925**, *108*, 105−111.
(6) Arndt, S.; Laugel, G.; Levchenko, S.; Horn, R.; Baerns, M.; Scheffler, M.; Schlögl, R.; Schomäcker, R. *Catal. Rev.: Sci. Eng.* **2011**, *53*, 424−514.
(7) Myrach, P.; Nilius, N.; Levchenko, S. V.; Gonchar, A.; Risse, T.; Dinse, K.-P.; Boatner, L. A.; Frandsen, W.; Horn, R.; Freund, H.-J.; Schlögl, R.; Scheffler, M. *ChemCatChem* **2010**, *2*, 854−862.
(8) Schröder, D.; Schwarz, H. *Proc. Natl. Acad. Sci. U. S. A.* **2008**, *105*, 18114−18119.
(9) Lersch, M.; Tilset, M. *Chem. Rev.* **2005**, *105*, 2471−2526.
(10) Lunsford, J. H. *Catal. Today* **2000**, *63*, 165−174.
(11) Lunsford, J. H. *Angew. Chem., Int. Ed. Engl.* **1995**, *34*, 970−980.
(12) Schwarz, H. *Chem. Phys. Lett.* **2015**, *629*, 91−101.
(13) Dietl, N.; Schlangen, M.; Schwarz, H. *Angew. Chem., Int. Ed.* **2012**, *51*, 5544−5555.
(14) Lai, W.; Li, C.; Chen, H.; Shaik, S. *Angew. Chem., Int. Ed.* **2012**, *51*, 5556−5578.
(15) Mayer, J. M. *J. Phys. Chem. Lett.* **2011**, *2*, 1481−1489.
(16) Janardanan, D.; Usharani, D.; Shaik, S. *Angew. Chem., Int. Ed.* **2012**, *51*, 4421−4425.
(17) Li, C.; Danovich, D.; Shaik, S. S. *Chem. Sci.* **2012**, *3*, 1903−1918.
(18) Geng, C. Y.; Ye, S.; Neese, F. *Angew. Chem., Int. Ed.* **2010**, *49*, 5717−5720.
(19) Li, J.; Zhou, S.; Zhang, J.; Schlangen, M.; Weiske, T.; Usharani, D.; Shaik, S.; Schwarz, H. *J. Am. Chem. Soc.* **2016**, *138*, 7973−7981.
(20) Hammes-Schiffer, S. *J. Am. Chem. Soc.* **2015**, *137*, 8860−8871.
(21) Siewert, I. *Chem. - Eur. J.* **2015**, *21*, 15078−15091.
(22) Saouma, C. T.; Mayer, J. M. *Chem. Sci.* **2014**, *5*, 21−31.
(23) Migliore, A.; Polizzi, N. F.; Therien, M. J.; Beratan, D. N. *Chem. Rev.* **2014**, *114*, 3381−3465.
(24) Savéant, J.-M. *Annu. Rev. Anal. Chem.* **2014**, *7*, 537−560.
(25) Layfield, J. P.; Hammes-Schiffer, S. *Chem. Rev.* **2014**, *114*, 3466−3494.
(26) Chen, X.; Ma, G.; Sun, W.; Dai, H.; Xiao, D.; Zhang, Y.; Qin, X.; Liu, Y.; Bu, Y. *J. Am. Chem. Soc.* **2014**, *136*, 4515−4524.
(27) Weinberg, D. R.; Gagliardi, C. J.; Hull, J. F.; Murphy, C. F.; Kent, C. A.; Westlake, B. C.; Paul, A.; Ess, D. H.; McCafferty, D. G.; Meyer, T. J. *Chem. Rev.* **2012**, *112*, 4016−4093.
(28) Cembran, A.; Provorse, M. R.; Wang, C.; Wu, W.; Gao, J. *J. Chem. Theory Comput.* **2012**, *8*, 4347−4358.
(29) Mayer, J. M. *Acc. Chem. Res.* **2011**, *44*, 36−46.
(30) Wenger, O. S. *Chem. - Eur. J.* **2011**, *17*, 11692−11702.

DOI: 10.1021/jacs.6b07246
J. Am. Chem. Soc. 2016, 138, 11368−11377

(31) Liu, S.; Ess, D. H.; Schauer, C. K. *J. Phys. Chem. A* **2011**, *115*, 4738−4742.
(32) Warren, J. J.; Tronic, T. A.; Mayer, J. M. *Chem. Rev.* **2010**, *110*, 6961−7001.
(33) Costentin, C.; Robert, M.; Savéant, J.-M. *Acc. Chem. Res.* **2010**, *43*, 1019−1029.
(34) Hammes-Schiffer, S. *Acc. Chem. Res.* **2009**, *42*, 1881−1889.
(35) Siegbahn, P. E. *Acc. Chem. Res.* **2009**, *42*, 1871−1880.
(36) Tishchenko, O.; Truhlar, D. G.; Ceulemans, A.; Nguyên, M. T. *J. Am. Chem. Soc.* **2008**, *130*, 7000−7010.
(37) Chen, X.; Bu, Y. *J. Am. Chem. Soc.* **2007**, *129*, 9713−9720.
(38) Meyer, T. J.; Huynh, M. H. V.; Thorp, H. H. *Angew. Chem., Int. Ed.* **2007**, *46*, 5284−5304.
(39) Huynh, M. H. V.; Meyer, T. J. *Chem. Rev.* **2007**, *107*, 5004−5064.
(40) Skone, J. H.; Soudackov, A. V.; Hammes-Schiffer, S. *J. Am. Chem. Soc.* **2006**, *128*, 16655−16663.
(41) Mayer, J. M. *Annu. Rev. Phys. Chem.* **2004**, *55*, 363−390.
(42) Mayer, J. M.; Hrovat, D. A.; Thomas, J. L.; Borden, W. T. *J. Am. Chem. Soc.* **2002**, *124*, 11142−11147.
(43) Hammes-Schiffer, S. *Acc. Chem. Res.* **2001**, *34*, 273−281.
(44) Cukier, R. I.; Nocera, D. G. *Annu. Rev. Phys. Chem.* **1998**, *49*, 337−369.
(45) Kwapien, K.; Paier, J.; Sauer, J.; Geske, M.; Zavyalova, U.; Horn, R.; Schwach, P.; Trunschke, A.; Schlögl, R. *Angew. Chem., Int. Ed.* **2014**, *53*, 8774−8778.
(46) Copéret, C. *Chem. Rev.* **2010**, *110*, 656−680.
(47) Sauer, J.; Freund, H.-J. *Catal. Lett.* **2015**, *145*, 109−125.
(48) Zavyalova, U.; Holena, M.; Schlögl, R.; Baerns, M. *ChemCatChem* **2011**, *3*, 1935−1947.
(49) Sinev, M. Y.; Fattakhova, Z. T.; Lomonosov, V. I.; Gordienko, Y. A. *J. Nat. Gas Chem.* **2009**, *18*, 273−287.
(50) Catlow, C. R. A.; French, S. A.; Sokol, A. A.; Thomas, J. M. *Philos. Trans. R. Soc., A* **2005**, *363*, 913−936 and references therein..
(51) Wu, M. C.; Truong, C. M.; Coulter, K.; Goodman, D. W. *J. Vac. Sci. Technol., A* **1993**, *11*, 2174−2178.
(52) Wu, M. C.; Truong, C. M.; Coulter, K.; Goodman, D. W. *J. Catal.* **1993**, *140*, 344−352.
(53) Wu, M.-C.; Truong, C. M.; Goodman, D. W. *Phys. Rev. B: Condens. Matter Mater. Phys.* **1992**, *46*, 12688−12694.
(54) Wu, M. C.; Truong, C. M.; Coulter, K.; Goodman, D. W. *J. Am. Chem. Soc.* **1992**, *114*, 7565−7567.
(55) Böhme, D. K.; Schwarz, H. *Angew. Chem., Int. Ed.* **2005**, *44*, 2336−2354.
(56) Schwarz, H. *Isr. J. Chem.* **2014**, *54*, 1413−1431.
(57) Lang, S. M.; Bernhardt, T. M. *Phys. Chem. Chem. Phys.* **2012**, *14*, 9255−9269.
(58) Schlangen, M.; Schwarz, H. *Catal. Lett.* **2012**, *142*, 1265−1278.
(59) Schwarz, H. *Angew. Chem., Int. Ed.* **2011**, *50*, 10096−10115.
(60) Roithová, J.; Schröder, D. *Chem. Rev.* **2010**, *110*, 1170−1211.
(61) Sperger, T.; Sanhueza, I. A.; Schoenebeck, F. *Acc. Chem. Res.* **2016**, *49*, 1311−1319.
(62) Corma, A. *Angew. Chem., Int. Ed.* **2016**, *55*, 6112−6113.
(63) O'Hair, R. A. J.; Rijs, N. J. *Acc. Chem. Res.* **2015**, *48*, 329−340.
(64) Roithová, J.; Schröder, D. *Coord. Chem. Rev.* **2009**, *253*, 666−677.
(65) Wischert, R.; Laurent, P.; Copéret, C.; Delbecq, F.; Sautet, P. *J. Am. Chem. Soc.* **2012**, *134*, 14430−14449.
(66) Balcells, D.; Clot, E.; Eisenstein, O. *Chem. Rev.* **2010**, *110*, 749−823.
(67) Werkema, E. L.; Maron, L.; Eisenstein, O.; Andersen, R. A. *J. Am. Chem. Soc.* **2007**, *129*, 2529−2541.
(68) Copéret, C.; Grouiller, A.; Basset, J.-M.; Chermette, H. *ChemPhysChem* **2003**, *4*, 608−611.
(69) Choudhary, V. R.; Rane, V. H.; Pandit, M. Y. *J. Chem. Technol. Biotechnol.* **1997**, *68*, 177−186.
(70) Schwarz, H. *Angew. Chem., Int. Ed.* **2015**, *54*, 10090−10100.
(71) Li, J.; Wu, X.-N.; Schlangen, M.; Zhou, S.; González-Navarrete, P.; Tang, S.; Schwarz, H. *Angew. Chem., Int. Ed.* **2015**, *54*, 5074−5078.
(72) Kwapien, K.; Sierka, M.; Döbler, J.; Sauer, J.; Haertelt, M.; Fielicke, A.; Meijer, G. *Angew. Chem., Int. Ed.* **2011**, *50*, 1716−1719.
(73) Schröder, D.; Roithová, J. *Angew. Chem., Int. Ed.* **2006**, *45*, 5705−5708.
(74) Kwapien, K.; Sierka, M.; Döbler, J.; Sauer, J. *ChemCatChem* **2010**, *2*, 819−826.
(75) Wischert, R.; Copéret, C.; Delbecq, F.; Sautet, P. *Angew. Chem., Int. Ed.* **2011**, *50*, 3202−3205.
(76) Joubert, J.; Salameh, A.; Krakoviack, V.; Delbecq, F.; Sautet, P.; Copéret, C.; Basset, J. M. *J. Phys. Chem. B* **2006**, *110*, 23944−23950.
(77) Wang, Z. C.; Dietl, N.; Kretschmer, R.; Ma, J. B.; Weiske, T.; Schlangen, M.; Schwarz, H. *Angew. Chem., Int. Ed.* **2012**, *51*, 3703−3707.
(78) Kummerlöwe, G.; Beyer, M. K. *Int. J. Mass Spectrom.* **2005**, *244*, 84−90.
(79) Su, T.; Bowers, M. T. *J. Chem. Phys.* **1973**, *58*, 3027−3037.
(80) Bowers, M. T.; Laudenslager, J. B. *J. Chem. Phys.* **1972**, *56*, 4711−4712.
(81) Heitz, S.; Epping, J.-D.; Aksu, Y.; Driess, M. *Chem. Mater.* **2010**, *22*, 4563−4571.
(82) Heitz, S.; Aksu, Y.; Merschjann, C.; Driess, M. *Chem. Mater.* **2010**, *22*, 1376−1385.
(83) Ding, X.-L.; Wu, X.-N.; Zhao, Y.-X.; He, S.-G. *Acc. Chem. Res.* **2012**, *45*, 382−390.
(84) Zhao, Y.-X.; Wu, X.-N.; Ma, J.-B.; He, S.-G.; Ding, X.-L. *Phys. Chem. Chem. Phys.* **2011**, *13*, 1925−1938.
(85) Li, J.; Wu, X.-N.; Zhou, S.; Tang, S.; Schlangen, M.; Schwarz, H. *Angew. Chem., Int. Ed.* **2015**, *54*, 12298−12302.
(86) Li, J.; Zhou, S.; Wu, X.-N.; Tang, S.; Schlangen, M.; Schwarz, H. *Angew. Chem., Int. Ed.* **2015**, *54*, 11861−11864.
(87) Usharani, D.; Lacy, D. C.; Borovik, A. S.; Shaik, S. *J. Am. Chem. Soc.* **2013**, *135*, 17090−17104.
(88) Usharani, D.; Janardanan, D.; Li, C.; Shaik, S. S. *Acc. Chem. Res.* **2013**, *46*, 471−482.
(89) van Zeist, W.-J.; Bickelhaupt, F. M. *Org. Biomol. Chem.* **2010**, *8*, 3118−3127.
(90) Ess, D. H.; Houk, K. N. *J. Am. Chem. Soc.* **2008**, *130*, 10187−10198.
(91) Legault, C. Y.; Garcia, Y.; Merlic, C. A.; Houk, K. N. *J. Am. Chem. Soc.* **2007**, *129*, 12664−12665.
(92) Ess, D. H.; Houk, K. N. *J. Am. Chem. Soc.* **2007**, *129*, 10646−10647.
(93) Diefenbach, A.; Bickelhaupt, F. M. *J. Phys. Chem. A* **2004**, *108*, 8460−8466.
(94) Mitchell, D. J.; Schlegel, H. B.; Shaik, S. S.; Wolfe, S. *Can. J. Chem.* **1985**, *63*, 1642−1648.
(95) Ziegler, T.; Rauk, A. *Inorg. Chem.* **1979**, *18*, 1558−1565.
(96) Strozier, R. W.; Caramella, P.; Houk, K. N. *J. Am. Chem. Soc.* **1979**, *101*, 1340−1343.
(97) Ziegler, T.; Rauk, A. *Theor. Chim. Acta* **1977**, *46*, 1−10.
(98) Kitaura, K.; Morokuma, K. *Int. J. Quantum Chem.* **1976**, *10*, 325−340.
(99) Morokuma, K. *J. Chem. Phys.* **1971**, *55*, 1236−1244.
(100) Sun, X.; Geng, C.; Huo, R.; Ryde, U.; Bu, Y.; Li, J. *J. Phys. Chem. B* **2014**, *118*, 1493−1500.
(101) Sun, X.; Sun, X.; Geng, C.; Zhao, H.; Li, J. *J. Phys. Chem. A* **2014**, *118*, 7146−7158.
(102) Li, J. L.; Zhang, X.; Huang, X. R. *Phys. Chem. Chem. Phys.* **2012**, *14*, 246−256.
(103) Sun, X. L.; Huang, X. R.; Li, J. L.; Huo, R. P.; Sun, C. C. *J. Phys. Chem. A* **2012**, *116*, 1475−1485.
(104) Fukui, K. *Science* **1982**, *218*, 747−754.
(105) Oda, A.; Torigoe, H.; Itadani, A.; Ohkubo, T.; Yumura, T.; Kobayashi, H.; Kuroda, Y. *J. Phys. Chem. C* **2014**, *118*, 15234−15241.
(106) Li, Z.-Y.; Zhao, Y.-X.; Wu, X.-N.; Ding, X.-L.; He, S.-G. *Chem. - Eur. J.* **2011**, *17*, 11728−11733.
(107) Engeser, M.; Weiske, T.; Schröder, D.; Schwarz, H. *J. Phys. Chem. A* **2003**, *107*, 2855−2859.

DOI: 10.1021/jacs.6b07246
J. Am. Chem. Soc. 2016, 138, 11368−11377

(108) Schröder, D.; Schwarz, H.; Clemmer, D. E.; Chen, Y.; Armentrout, P. B.; Baranov, V. I.; Böhme, D. K. *Int. J. Mass Spectrom. Ion Processes* **1997**, *161*, 175−191.
(109) Eller, K.; Schwarz, H. *Int. J. Mass Spectrom. Ion Processes* **1989**, *93*, 243−257.
(110) Ding, X.-L.; Li, Z.-Y.; Meng, J.-H.; Zhao, Y.-X.; He, S.-G. *J. Chem. Phys.* **2012**, *137*, 214311.
(111) Becke, A. D. *J. Chem. Phys.* **1993**, *98*, 5648−5652.
(112) Lee, C.; Yang, W.; Parr, R. G. *Phys. Rev. B: Condens. Matter Mater. Phys.* **1988**, *37*, 785−789.
(113) Zhang, J.; Dolg, M. *Phys. Chem. Chem. Phys.* **2016**, *18*, 3003−3010.
(114) Zhang, J.; Dolg, M. *Phys. Chem. Chem. Phys.* **2015**, *17*, 24173−24181.
(115) Řezáč, J.; Hobza, P. *J. Chem. Theory Comput.* **2014**, *10*, 3066−3073.
(116) Karton, A.; Tarnopolsky, A.; Lamère, J.-F.; Schatz, G. C.; Martin, J. M. L. *J. Phys. Chem. A* **2008**, *112*, 12868−12886.
(117) Grimme, S. *J. Chem. Phys.* **2006**, *124*, 034108.
(118) Truhlar, D. G.; Gordon, M. S. *Science* **1990**, *249*, 491−498.
(119) Gonzalez, C.; Schlegel, H. B. *J. Phys. Chem.* **1990**, *94*, 5523−5527.
(120) Fukui, K. *Acc. Chem. Res.* **1981**, *14*, 363−368.
(121) Fukui, K. *J. Phys. Chem.* **1970**, *74*, 4161−4163.
(122) Reed, A. E.; Curtiss, L. A.; Weinhold, F. A. *Chem. Rev.* **1988**, *88*, 899−926.
(123) Carpenter, J. E.; Weinhold, F. A. *J. Mol. Struct.: THEOCHEM* **1988**, *169*, 41−62.
(124) Reed, A. E.; Weinstock, R. B.; Weinhold, F. A. *J. Chem. Phys.* **1985**, *83*, 735−746.
(125) Reed, A. E.; Weinhold, F. A. *J. Chem. Phys.* **1985**, *83*, 1736−1740.
(126) Reed, A. E.; Weinhold, F. A. *J. Chem. Phys.* **1983**, *78*, 4066−4073.
(127) Foster, J. P.; Weinhold, F. A. *J. Am. Chem. Soc.* **1980**, *102*, 7211−7218.
(128) Usharani, D.; Lai, W.; Li, C.; Chen, H.; Danovich, D.; Shaik, S. *Chem. Soc. Rev.* **2014**, *43*, 4968−4988.
(129) Frisch, M. J.; Trucks, G. W.; Schlegel, H. B.; Scuseria, G. E.; Robb, M. A.; Cheeseman, J. R.; Scalmani, G.; Barone, V.; Mennucci, B.; Petersson, G. A.; Nakatsuji, H.; Caricato, M.; Li, X.; Hratchian, H. P.; Izmaylov, A. F.; Bloino, J.; Zheng, G.; Sonnenberg, J. L.; Hada, M.; Ehara, M.; Toyota, K.; Fukuda, R.; Hasegawa, J.; Ishida, M.; Nakajima, T.; Honda, Y.; Kitao, O.; Nakai, H.; Vreven, T.; J. A. Montgomery, J.; Peralta, J. E.; Ogliaro, F.; Bearpark, M.; Heyd, J. J.; Brothers, E.; Kudin, K. N.; Staroverov, V. N.; Keith, T.; Kobayashi, R.; Normand, J.; Raghavachari, K.; Rendell, A.; Burant, J. C.; Iyengar, S. S.; Tomasi, J.; Cossi, M.; Rega, N.; Millam, J. M.; Klene, M.; Knox, J. E.; Cross, J. B.; Bakken, V.; Adamo, C.; Jaramillo, J.; Gomperts, R.; Stratmann, R. E.; Yazyev, O.; Austin, A. J.; Cammi, R.; Pomelli, C.; Ochterski, J. W.; Martin, R. L.; Morokuma, K.; Zakrzewski, V. G.; Voth, G. A.; Salvador, P.; Dannenberg, J. J.; Dapprich, S.; Daniels, A. D.; Farkas, O.; Foresman, J. B.; Ortiz, J. V.; Cioslowski, J.; Fox, D. J. *Gaussian 09*, Revision D.01; Gaussian, Inc.: Wallingford CT, 2013.
(130) Werner, H.-J.; Knowles, P. J.; Knizia, G.; Manby, F. R.; Schütz, M.; Celani, P.; Korona, T.; Lindh, R.; Mitrushenkov, A.; Rauhut, G.; Shamasundar, K. R.; Adler, T. B.; Amos, R. D.; Bernhardsson, A.; Berning, A.; Cooper, D. L.; Deegan, M. J. O.; Dobbyn, A. J.; Eckert, F.; Goll, E.; Hampel, C.; Hesselmann, A.; Hetzer, G.; Hrenar, T.; Jansen, G.; Köppl, C.; Liu, Y.; Lloyd, A. W.; Mata, R. A.; May, A. J.; McNicholas, S. J.; Meyer, W.; Mura, M. E.; Nicklass, A.; O'Neill, D. P.; Palmieri, P.; Peng, D.; Pflüger, K.; Pitzer, R.; Reiher, M.; Shiozaki, T.; Stoll, H.; Stone, A. J.; Tarroni, R.; Thorsteinsson, T.; Wang, M. *Molpro: A Package of Ab Initio Programs*, version 2012.1; http://www.molpro.net.

DOI: 10.1021/jacs.6b07246
J. Am. Chem. Soc. 2016, 138, 11368−11377